THE ROLL OF s AND t UNITARITY SCREENING IN POMERON PHYSICS*

Uri Maor

Department of Particle Physics, School of Physics and Astronomy
Raymond and Beverly Sackler Faculty of Exact Science, Tel Aviv University
Tel Aviv, 69978, Israel

(Received November 2, 2011)

Dedicated to Andrzej Białas in honour of his 75th birthday

An updated formulation of the soft Pomeron, in which s and t channel unitarity screenings are included, is reviewed. The consequent soft scattering features are explored. A summary of the cross-section outputs of the leading groups active in this research are presented including also the calculated values of the gap survival probabilities, which is relevant, mostly, to hard diffractive processes. A utilization of pQCD in soft Pomeron formulation based on Gribov's Reggeon calculus is applied in the GLM model. The output parameters are compatible with AdS/CFT correspondence. The interplay between Pomeron theory and its corresponding data analysis is discussed. LHC soft scattering data is quoted and compared with theoretical predictions. Its implications for the Pomeron model are discussed.

DOI:10.5506/APhysPolB.42.2547
PACS numbers: 13.85.–t, 13.85.Hd, 11.55.–m, 11.55.Bq

1. Introduction

Hard QCD deals with the strong interactions of high transverse momenta partons. These are short distance phenomena which are calculated within the framework of pQCD. Soft QCD is traditionally associated with low transverse momenta partons separated by large distances, for which we are unable to utilize perturbative methods. The relevant npQCD calculations are, thus, based on phenomenological models, foremost, the Regge pole model in which the Pomeron ($I\!P$) is the leading term. As such, $I\!P$ exchange dominates the soft scattering dynamics at the Tevatron and above.

* Presented at the LI Cracow School of Theoretical Physics "Soft Side of the LHC", Zakopane, Poland, June 11–19, 2011.

The original Pomeron, with $\alpha_{I\!P}(0) = 1$, was postulated [1] as an added phenomenological feature to the Regge model. Theoretically, it is induced by Gribov's Reggeon Calculus [2]. The total and elastic (but NOT diffractive) cross-sections in the ISR–Tevatron range are well reproduced by the simple DL parametrization [3] where,

$$\alpha_{I\!P}(t) = 1 + \Delta_{I\!P} + \alpha'_{I\!P} t \,, \tag{1.1}$$

in which $\Delta_{I\!P} = 0.08$ and $\alpha'_{I\!P} = 0.25$ GeV^{-2}.

The simple Pomeron model needs considerable re-formulations at high energies, so as to be compatible with s and t unitarity. This procedure is executed in impact parameter b-space. I shall use a normalization, where

$$\frac{d\sigma_{\rm el}}{dt} = \pi \mid f_{\rm el}(s,t) \mid^2 \,, \tag{1.2}$$

$$\sigma_{\rm tot} = 4\pi {\rm Im} f_{\rm el}(s,0) \,. \tag{1.3}$$

The b-space elastic amplitude is defined as the transform

$$a_{\rm el}(s,b) = \frac{1}{2\pi} \int dq e^{-i\boldsymbol{q}\cdot\boldsymbol{b}} f_{\rm el}(s,t) \tag{1.4}$$

in which $t = -\boldsymbol{q}^2$. We obtain

$$\sigma_{\rm tot} = 2 \int d^2 b \, {\rm Im}\, a_{\rm el}(s,b) \,, \tag{1.5}$$

$$\sigma_{\rm el} = \int d^2 b \mid a_{\rm el}(s,b) \mid^2 \,. \tag{1.6}$$

In this paper I shall briefly review the transition from the original definition of the Regge Pomeron to its present formulation, with special attention to LHC physics. The present vigorous studies of the $I\!P$ and its dynamics are based on sophisticated utilizations of ideas dated decades ago.

- S-Matrix Regge Poles: Regge (1957), Chew–Frautchi (1960).
- Reggeon Field Theory: Gribov (1962, 1968).
- Eikonal Model: Glauber (1959).
- GW Proton Wave Function Decomposition: Good–Walker (1960).
- Triple Pomeron Formalism: Mueller (1971).
- Multi Pomeron Interactions: Gribov (1968), Kaidalov *et al.* (1986).
- Pomeron as a 2 gluon color singlet: Low (1975), Nussinov (1975).
- BFKL hard Pomeron: Balitsky–Fadin–Kuraev–Lipatov (1975–1978).

Updated $I\!P$ models have radically changed our perception of the Regge Pomeron. They are specified by an elaborate multi component architecture.

- Bare non-screened $I\!P$ amplitudes in a 2 channel Good–Walker (GW) system composed of elastic and "low mass" diffraction.
- Eikonal re-scatterings of the incoming projectiles secure that the scattering amplitudes are bounded by s-channel unitarity black disc bound.
- t-channel unitarity, induced by multi $I\!P$ interactions, leads to "high mass" diffraction and additional screening of the GW sector.
- The survival probability factor, which has eikonal and multi $I\!P$ components, induces a reduction of the non-GW diffraction.

Current $I\!P$ models are coupled to a price tag of relatively large $\Delta_{I\!P}$ and exceedingly small $\alpha'_{I\!P}$, which seemingly destroy the conventional features of the Regge Pomeron in which the s dependence of a $I\!P$ exchange amplitude is determined by $\Delta_{I\!P}$ and the shrinkage of its t-dependence slope by $\alpha'_{I\!P}$. As we shall see, the traditional Regge features are restored by s and t unitarity screenings.

The first part of this paper is devoted to a brief description of the components of the updated $I\!P$ models. In the second part I shall focus on the predictions obtained from these models with special attention to the new LHC results on soft QCD and their implications on $I\!P$ physics at exceedingly high energies.

2. s-channel unitarity

If the Pomeron is super critical ($\Delta_{I\!P} > 0$), $\sigma_{\rm el}$ grows indefinitely faster than $\sigma_{\rm tot}$ and will, eventually, get larger! This paradox is eliminated by imposing an s-unitarity bound on $a_{\rm el}(s,b)$. Enforcing unitarity is model dependent, so I shall start with the simplest diagonal re-scattering matrix, where repeated elastic re-scatterings secure s-channel unitarity.

$$2\,{\rm Im}\,a_{\rm el}(s,b) =\mid a_{\rm el}(s,b)|^2 + G^{\rm in}(s,b)\,. \tag{2.7}$$

This is no more than a statement that $\sigma_{\rm tot}(s,b) = \sigma_{\rm el}(s,b) + \sigma_{\rm in}(s,b)$. Its general solution is

$$a_{\rm el}(s,b) \;=\; i\left(1 - e^{-\Omega(s,b)/2}\right)\,, \tag{2.8}$$

$$G^{\rm in}(s,b) \;=\; 1\; - e^{-\Omega(s,b)}\,, \tag{2.9}$$

in which $\Omega(s,b)$ is arbitrary. We obtain a unitarity bound of $\mid a_{\rm el}(s,b)\mid\leq 2$. In a Glauber type eikonal approximation, the input opacity $\Omega(s,b)$ is real, *i.e.* $a_{\rm el}(s,b)$ is imaginary. It equals the imaginary part of the input Born term, a $I\!P$ exchange amplitude in our context. The output bound is

$$\mid a_{\rm el}(s,b) \mid \leq 1\,, \tag{2.10}$$

which is the black disc bound. Analyticity and crossing symmetry are restored by the dispersion relation substitution $s^{\alpha_{I\!P}} \rightarrow s^{\alpha_{I\!P}} e^{-\frac{1}{2}i\pi\alpha_{I\!P}}$.

Total, elastic and inelastic cross-sections are

$$\sigma_{\rm tot} \;=\; 2\int d^2b \left(1\;-\;e^{-\Omega(s,b)/2}\right)\,, \tag{2.11}$$

$$\sigma_{\rm el} \;=\; \int d^2b \left(1\;-\;e^{-\Omega(s,b)/2}\right)^2\,, \tag{2.12}$$

$$\sigma_{\rm in} \;=\; \int d^2b \left(1\;-\;e^{-\Omega(s,b)}\right)\,. \tag{2.13}$$

Imposing unitarity + analyticity/crossing bounds leads to the Froissart bound

$$\sigma_{\rm tot} \leq C \ln^2(s/s_0)\,, \tag{2.14}$$

in which $C \;\propto\; 1/m_{\pi}^2$. This is a numerical (not a functional) bound. Its value is far too high to provide a useful bound. There have been suggestions to replace the pion mass with a gluonium mass. However, these ideas, as appealing as they may be, lack a sound base. Fig. 1 illustrates the s-unitarity bounds and the suppressed scattering amplitude output.

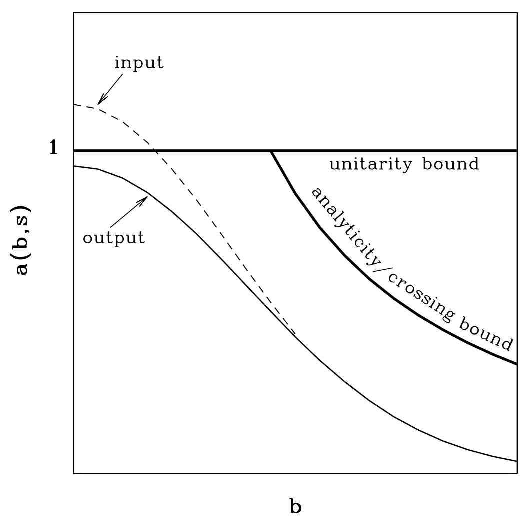

Fig. 1. The effect of eikonal screening restoring s unitarity. The bounds implied by analiticity/crossing are also shown.

3. Good–Walker eikonal models

Current eikonal models are two channel, including both elastic and diffractive re-scatterings of the initial projectiles. This is a consequence of the GW mechanism [4] in which the proton (anti-proton) wave function has elastic and diffractive components. However, models based on just the GW mechanism reproduce the total and elastic cross-sections well, but fail to describe the complete diffractive cross-section data. Theoretically [5], these deficiencies can be eliminated by the introduction of multi $I\!\!P$ interactions leading to high mass diffraction. These "Pomeron-enhanced" contributions, are derived from Gribov's Reggeon calculus [2]. The zero order, on which these calculations are based, is Mueller's triple Pomeron high mass SD formalism [6].

Consider a $I\!\!P$ vertex with an incoming hadron $|h\rangle$ and outgoing diffractive system approximated [7] as a single state $|D\rangle$. The GW mechanism is based on the observation that these states do not diagonalize the 2×2 interaction matrix. We denote the interaction matrix eigenstates by ψ_1 and ψ_2. The wave functions of the incoming hadron and outgoing diffractive state are

$$\psi_h = \alpha\,\psi_1 + \beta\,\psi_2\,, \tag{3.15}$$
$$\psi_D = -\beta\,\psi_1 + \alpha\,\psi_2\,, \tag{3.16}$$

where, $\alpha^2 + \beta^2 = 1$. For each of the four independent elastic scattering amplitudes $A^{\mathrm{S}}_{i,k}(s,b)$ we write its elastic unitarity equation

$$\mathrm{Im}\,A^{\mathrm{S}}_{i,k}(s,b) = \left|A^{\mathrm{S}}_{i,k}(s,b)\right|^2 + G^{\mathrm{in}}_{i,k}(s,b)\,, \tag{3.17}$$

in which

$$A^{\mathrm{S}}_{i,k}(s,b) = i\left(1-\exp\left(-\tfrac{1}{2}\Omega^{\mathrm{S}}_{i,k}(s,b)\right)\right)\,, \tag{3.18}$$
$$G^{\mathrm{in}}_{i,k}(s,b) = \left(1-\exp\left(-\Omega^{\mathrm{S}}_{i,k}(s,b)\right)\right)\,. \tag{3.19}$$

$G^{\mathrm{in}}_{i,k}$ is the summed probability for all non-GW induced inelastic final states. From Eq. (3.19) we deduce that

$$P^{\mathrm{S}}_{i,k}(s,b) = \exp\left(-\Omega^{\mathrm{S}}_{i,k}(s,b)\right)\,, \tag{3.20}$$

is the probability that the GW (i,k) projectiles will reach the final Large Rapidity Gap (LRG) interaction in their initial state, regardless of their prior re-scatterings.

For p–p and $\bar{p}$–p scattering $A^{\rm S}_{1,2} = A^{\rm S}_{2,1}$, which reduces the number of independent amplitudes to three. The corresponding elastic, SD and DD amplitudes are

$$a_{\rm el}(s,b) = i\left\{\alpha^4 A^{\rm S}_{1,1} + 2\alpha^2\beta^2 A^{\rm S}_{1,2} + \beta^4 \mathcal{A}^{\rm S}_{2,2}\right\}, \tag{3.21}$$

$$a_{\rm sd}(s,b) = i\alpha\beta\left\{-\alpha^2 A^{\rm S}_{1,1} + (\alpha^2-\beta^2) A^{\rm S}_{1,2} + \beta^2 A^{\rm S}_{2,2}\right\}, \tag{3.22}$$

$$a_{\rm dd} = i\alpha^2\beta^2\left\{A^{\rm S}_{1,1} - 2A^{\rm S}_{1,2} + A^{\rm S}_{2,2}\right\}. \tag{3.23}$$

For more details see Ref. [8] and references therein.

Eikonal models based on the GW mechanism use a Regge like formalism in which the opacity is

$$\Omega^{\rm S}_{i,k}(s,b) = \nu^{\rm S}_{i,k}(s)\Gamma^{\rm S}_{i,k}(s,b,\alpha'_{I\!P}). \tag{3.24}$$

$\nu^{\rm S}_{i,k}(s) = g_i g_k(\frac{s}{s_0})^{\Delta_{I\!P}}$. $\Gamma^{\rm S}_{i,k}$ are the b-space profiles, constructed so as to reproduce the differential $\frac{d\sigma}{dt}$ cross-sections in the elastic, SD and DD channels. In GLM $\Gamma^{\rm S}_{i,k}$ are given as the b-transforms of two t-poles expressions ($t=-q^2$). Setting $\alpha'_{I\!P}=0$, these profiles are energy independent

$$\frac{1}{(1+q^2/m_i^2)^2} \times \frac{1}{(1+q^2/m_k^2)^2} \Longrightarrow \Gamma^{\rm S}\left(b; m_i, m_k; \alpha'_{I\!P}=0\right). \tag{3.25}$$

GLM introduce a small energy dependence

$$m_i^2 \Longrightarrow m_i^2(s) \equiv \frac{m_i^2}{1 + 4m_i^2\alpha'_{I\!P}\ln(s/s_0)}. \tag{3.26}$$

The normalization and constraints on the large b behavior of the profiles, are determined by the data analysis. The above parametrization is compatible with the requirements of analyticity/crossing symmetry at large b, pQCD at large q^2 and Regge at small t. For details see Ref. [8].

4. Multi Pomeron interactions

Mueller applied [6] 3 body unitarity to equate the cross-section of

$$a + b \to M + b \tag{4.27}$$

to the triple Regge diagram

$$a + b + \bar{b} \to a + b + \bar{b}. \tag{4.28}$$

The core of this representation is a triple vertex with a leading $3I\!\!P$ term (see Fig. 2). The equation is valid for $\frac{m_p}{M^2} \ll 1$ and $\frac{M^2}{s} \ll 1$, defining "high mass diffraction". The corresponding cross-section is

$$M^2 \frac{d\sigma^{3I\!\!P}}{dt\, dM^2} = \frac{g_p^2(t) g_p(0) G_{3I\!\!P}}{16\,\pi^2} \left(\frac{s}{M^2}\right)^{2\alpha_{I\!\!P}(t)-2} \left(\frac{M^2}{s_0}\right)^{\alpha_{I\!\!P}(0)-1} . \tag{4.29}$$

Eq. (4.29) implies a correlation between the s dependences of the elastic and diffractive amplitudes and the mass dependence of the "high mass" SD amplitude. The procedure just described can be extended also to DD.

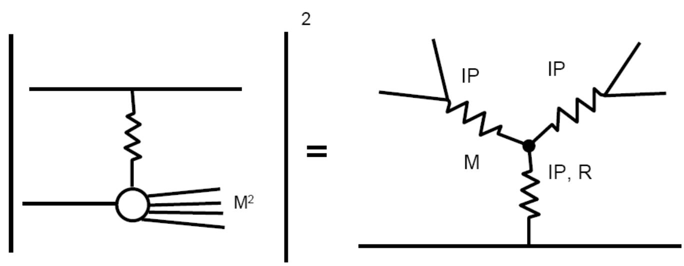

Fig. 2. Mueller's $3I\!\!P$ approximation for SD.

Provided $G_{3I\!\!P}$ is not too small, Muller's $3I\!\!P$ approximation for "high mass" single diffraction is the lowest order of a very large family of multi Pomeron interactions which are not included in the GW mechanism. This dynamical feature is compatible with t-channel unitarity. Fig. 3 shows the low order $I\!\!P$ Green's function. We distinguish between: (a) Enhanced diagrams which renormalize (in low order) the $I\!\!P$ propagator; (b) Semi-enhanced diagrams which renormalize (in low order) the p–$I\!\!P$–p vertexes. The complexity of these diagrams requires summing algorithms which are model dependent.

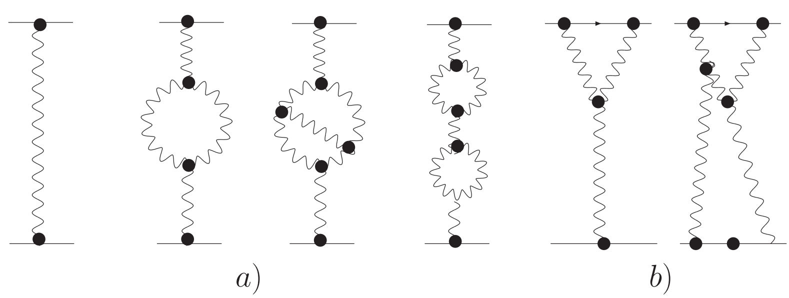

Fig. 3. The low order $I\!\!P$ Green's function.

Multi $I\!\!P$ interactions induce further screening of both the GW sector through $I\!\!P$ renormalization, and the non-GW sector through the corresponding gap survival probability (discussed in the next section).

The introduction of multi $I\!\!P$ interactions as a major component of the Pomeron model, poses a serious problem in as much as it depends on many unknown rapidity space point like couplings corresponding to $nI\!\!P \to mI\!\!P$. There are two optional procedures to overcome this difficulty:

1. In the GLM model [8] the microscopic sub structure of the Pomeron is provided by Gribov partonic interpretation of Regge theory, in which the slope of the Pomeron trajectory is related to the mean transverse momentum of the partonic dipoles constructing the Pomeron, and, consequently, the running QCD coupling constant.

$$\alpha'_{I\!\!P} \propto 1/\langle p_{\rm t}\rangle^2\,, \tag{4.30}$$

$$\alpha_{\rm S} \propto \pi/\ln\left(\langle p_{\rm t}^2\rangle/\Lambda^2_{\rm QCD}\right) \ll 1\,. \tag{4.31}$$

   GLM utilize the pQCD MPSI procedure [9], where $nI\!\!P \to mI\!\!P$ reduces to a sequence of $G_{3I\!\!P}$ vertexes (Fan diagrams), *i.e.* $2I\!\!P \to I\!\!P$ and $I\!\!P \to 2I\!\!P$.
2. In an alternative approach, KMR [10] assumed a recurrence relation for multi $I\!\!P$ couplings,

$$g^n_m = \tfrac{1}{2}\,g_N\,nm\,\lambda^{n+m-2} = \tfrac{1}{2}\,nm\,G_{3I\!\!P}\,\lambda^{n+m-3}\,. \tag{4.32}$$

   λ is a free parameter, $n+m > 2$, $G_{3I\!\!P} = \lambda g_N$. Kaidalov and Poghosyan (KP) [11] and Ostapchenko (Os) [12] have a similar coupling with a different normalization.

The need for s-channel screening of the bare $I\!\!P$ exchange amplitude has been recognized and integrated into phenomenological models long ago. The realization of t-channel multi $I\!\!P$ interaction is as old, but its full formulation and integration into the analysis of high energy soft interactions is relatively young. One of the main goals of this presentation is to emphasize the role of multi $I\!\!P$ interactions in high energy soft scattering and identify its experimental signatures.

5. LRG survival probability

The Pomeron is defined as a moving Regge pole void of electric and color charges. The proposition by Low and Nussinov [13] that the $I\!\!P$ is a 2 gluon color singlet, is intuitively appealing. This is a Born term description. In high order the 2 gluons are replaced by a gluonic ladder. The coupled experimental signature, indicating a diffractive process, is a large rapidity (in practice, pseudorapidity) gap (LRG) devoid of hadrons in the η–ϕ Lego plot,

$$\eta = -\ln\left(\tan\frac{\theta}{2}\right) . \tag{5.33}$$

Consider non-GW diffraction (soft or hard). This channel is contained in $G^{\rm in}_{i,k}$, rather than within the $A^{\rm S}_{i,k}$ GW amplitudes. The reduction of the bare non-screened non-GW diffractive cross-section is expressed by the probability that its rapidity gap signature will not be filled by partonic and/or hadronic debris originating from s and t channel screenings. This is expressed by the LRG survival probability factor.

The LHC experimental program is focused, to a considerable extent, on the discovery of the Higgs boson. I shall confine my discussion on this subject to a Standard Model Higgs with a relatively low mass of 120–180 GeV, produced in an exclusive central diffraction,

$$p + p \to p + \mathrm{LRG} + H + \mathrm{LRG} + p\,. \tag{5.34}$$

The advantage of this channel is that it has a distinctive signature of two large rapidity gaps and a favorable signal to background ratio, which is improved when the forward protons are tagged. The same mechanism is applied to di-jets and χ mesons central production. Denote the gap survival factor initiated by s-channel soft eikonalization $S^2_{\rm eik}$, and the one initiated by t-channel multi $I\!\!P$ interactions by $S^2_{\rm enh}$. Even though S^2 is obtained through a convolution of the s and t channel screenings (see Fig. 4), it can be reasonably well approximated through a factorization of the s-channel eikonal screening and the t-channel enhanced $I\!\!P$ screening.

$$S^2 = \frac{\sigma^{\rm scr}_{\rm diff}}{\sigma^{\rm nonscr}_{\rm diff}} \approx S^2_{\rm eik}\cdot S^2_{\rm enh}\,. \tag{5.35}$$

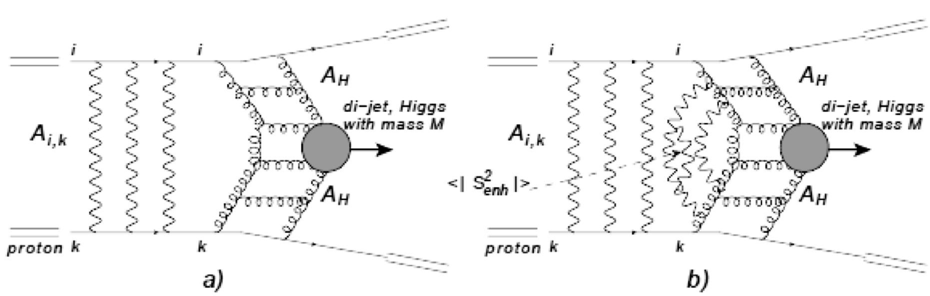

Fig. 4. An example of the screenings generating the gap survival probability for exclusive central diffractive production of the Higgs boson. (a) shows the contribution to the survival probability in the GW mechanism, while (b) illustrates the origin of the additional factor $\langle|S^2_{\rm enh}|\rangle$.

In a single channel eikonal model,

$$S^2_{\rm eik} = \frac{\int d^2b \mid M^{\rm in}_{\rm diff}(s,b) \mid^2 P^{\rm S}(s,b)}{\int d^2b \mid M^{\rm in}_{\rm diff}(s,b) \mid^2}\,. \tag{5.36}$$

Recall that, $G^{\rm in} = 1 - P^{\rm S}$, where, $P^{\rm S}(s,b) = e^{-\Omega_{I\!P}(s,b)}$. It is the probability that the colliding projectiles reach the $I\!P$ exchange diffractive reaction in their initial state, regardless of their prior re-scatterings. The calculation of $S^2_{\rm eik}$ in a multi channel model is straightforward, depending on the summation over the GW eigen states. It is coherent for an exclusive channel such as

$$p + p \to p + {\rm LRG} + {\rm Higgs} + {\rm LRG} + p\,, \tag{5.37}$$

and non-coherent for an inclusive channel such as

$$p + p \to X + {\rm LRG} + {\rm Higgs} + {\rm LRG} + Y\,. \tag{5.38}$$

As I have just noted, a precise calculation of S^2 requires a convolution of the s-channel eikonal initial re-scatterings of the incoming projectiles and the t-channel multi $I\!P$ interactions. A scheme of these diagrams in the GLM model is given in Fig. 5. The corresponding S^2 results [14] for exclusive central diffraction are presented in Fig. 6.

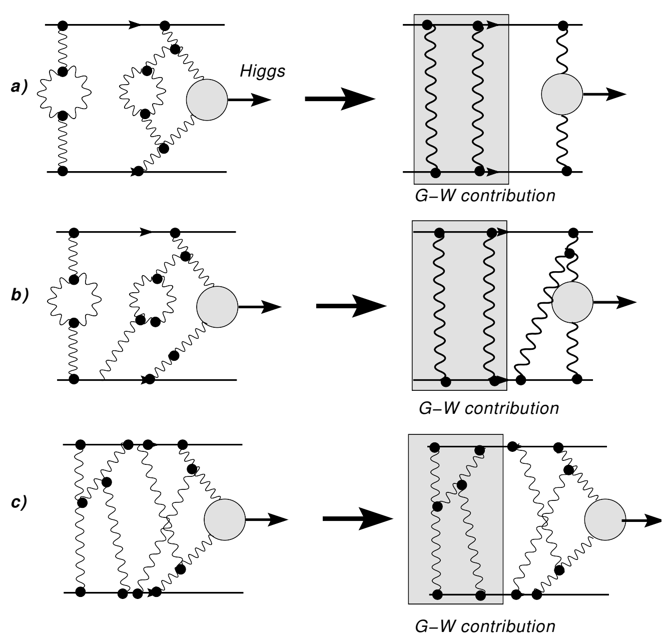

Fig. 5. GLM diagrams for exclusive central diffraction.

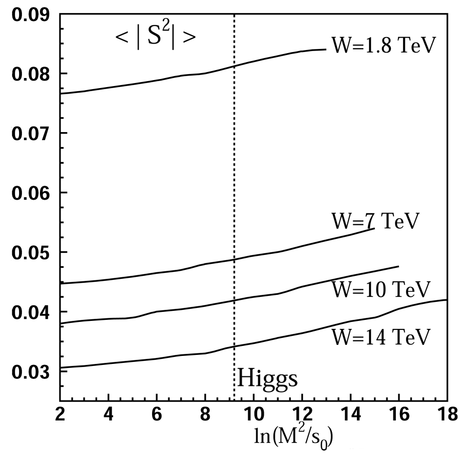

Fig. 6. GLM estimates of S^2 for exclusive central diffraction.

The s and t screenings induce a monotonous decrease of $\Delta_{I\!P}^{\rm eff}$ referred to as "$I\!P$ renormalization". Its GLM predictions are shown in Table I.

TABLE I

GLM $\Delta_{I\!P}^{\rm eff}$ in two energy ranges.

W[TeV]	$1.8 \to 14.0$	$14.0 \to 100.0$
$\Delta_{I\!P}^{\rm input} = 0.335$	0.056	0.041
$\Delta_{I\!P}^{\rm input} = 0.200$	0.074	0.060

6. How many Pomerons?

Following I shall discuss mostly multi channel $I\!P$ models in which s and t unitarity screenings are incorporated. The models are very similar conceptually, but differ in the details of their $I\!P$ model, multi $I\!P$ diagram summation procedures and data analyses.

- GLM (Tel Aviv): have a single soft $I\!P$ with hard characteristics [8]. $\Delta_{I\!P} = 0.20$ and $\alpha'_{I\!P} = 0.02$ GeV^{-2}. The GLM $I\!P$ does not depend on $k_{\rm t}$.
- KMR (Durham): have a BFKL like single soft $I\!P$ [10]. $\Delta_{I\!P} = 0.3$ and $\alpha'_{I\!P} \propto 1/p_{\rm t}^2$ depends on $k_{\rm t}$ evolution which determines the continuous value of $\alpha'_{I\!P}$.
- Os (Bergen): has 2 Pomerons [12]. Following are his set C parameters: Soft $I\!P$: $\Delta_{I\!P} = 0.17$ and $\alpha'_{I\!P} = 0.11$ GeV^{-2}. Hard $I\!P$: $\Delta_{I\!P} = 0.31$ and $\alpha'_{I\!P} = 0.085$ GeV^{-2}.

- KP (Moscow): is a single channel non-GW $I\!\!P$ model with a single, DL-like, soft $I\!\!P$ and 3 Regge secondary trajectories [11]. $\Delta_{I\!\!P} = 0.117$ and $\alpha'_{I\!\!P} = 0.252$ GeV^{-2}. $\Delta_f = 0.17$ and $\alpha'_f = 0.8$ GeV^{-2}; $\Delta_\rho = 0.5$ and $\alpha'_\rho = 0.9$ GeV^{-2}; $\Delta_\omega = 0.4$ and $\alpha'_\omega = 0.9$ GeV^{-2}.

pQCD study of e–p DIS, in the limit of very high Q^2 and exceedingly small x, led Balitsky, Fadin, Kuraev and Lipatov (1975–78) to introduce the hard BFKL Pomeron corresponding, in its lowest order to a hard gluon ladder. Note that, the soft $I\!\!P$ is a simple moving pole in the J-plane, while, the BFKL $I\!\!P$ is a branch cut. Commonly, though, the BFKL $I\!\!P$ is parameterized as a simple J-pole with parameters obtained from NLL resumed BFKL equation. $\Delta_{\rm BFKL} = 0.2$–0.35 and $\alpha'_{\rm BFKL} = 0$. These values are regarded as the signatures of the hard $I\!\!P$. Recall that, in pQCD the BFKL Pomeron slope $\alpha'_{I\!\!P} \propto 1/Q_{\rm s}^2 \to 0$ as $s \to \infty$. $Q_{\rm s}^2$ is the saturation scale.

The experimental study of e–p DIS provides a "laboratory" in which we can investigate the Pomeron properties as a function of its kinematic variables. Indeed, HERA e–p DIS data is a rich source of information on the $I\!\!P$ features. Fig. 7 presents the Q^2 dependence of $\Delta_{I\!\!P}^{\rm eff}$ obtained from DIS $\sigma(\gamma^* + p \to p + X) \propto s^\lambda$, $\lambda = \Delta_{I\!\!P}^{\rm eff}$. Fig. 7 clearly shows the smooth transition from the soft (non-perturbative) Pomeron to the hard (perturbative) Pomeron. As seen, at very small Q^2, $\Delta_{I\!\!P}^{\rm eff} \simeq 0.1$, is compatible with the

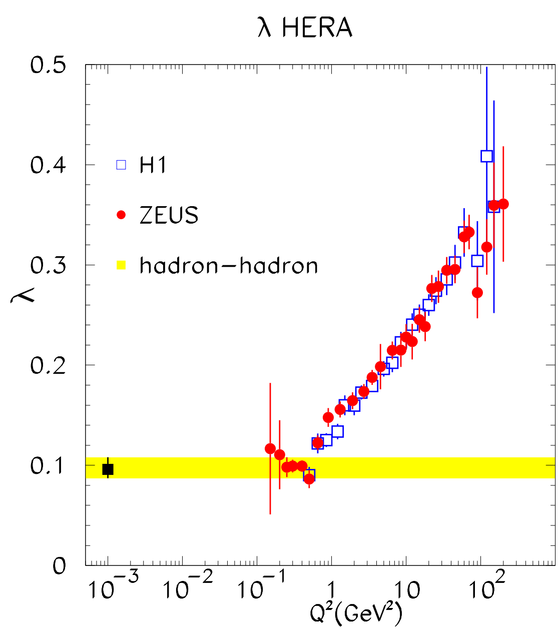

Fig. 7. Q^2 dependence of e–p DIS.

hadronic effective soft $I\!P$. At higher Q^2, up to $\simeq 200$ GeV^2, $\Delta_{I\!P}$ grows toward $\Delta_{I\!P}^{\rm eff} \simeq 0.35$, compatible with the DIS hard $I\!P$. The smooth transition from soft to hard $I\!P$ supports GLM and KMR choice of a single Pomeron.

There is an inherent difficulty in the leading concept of GLM and KMR who calculate the elastic and diffractive channels simultaneously. This approach requires a sum over all orders (loops) of the multi $I\!P$ interactions. Since there is no rigorous method to calculate the sum of the enhanced and semi-enhanced diagrams, both groups had to rely on approximations which are difficult to assess critically. Recall that GLM and KMR fix $\alpha'_{I\!P} = 0$. This implies a bound of validity for both models approximately $W = 100$ TeV.

GLM try to by-pass this problem by constructing a model [8, 14] based on the postulates stemmed from $N = 4$ SYM and pQCD.

- Following Ref. [16] $\alpha'_{I\!P} = 0$. From the information on multi-particle production at HERA [16] and early LHC (see the last section in this presentation) we estimate that $\lambda = 5$–9. Consequently, $\Delta_{I\!P} = 1 - 2/\sqrt{\lambda} \approx 0.11$–$0.33$. Fig. 8 shows the transition from the $N = 4$ SYM trajectory to the pQCD trajectory at $t = 0$.

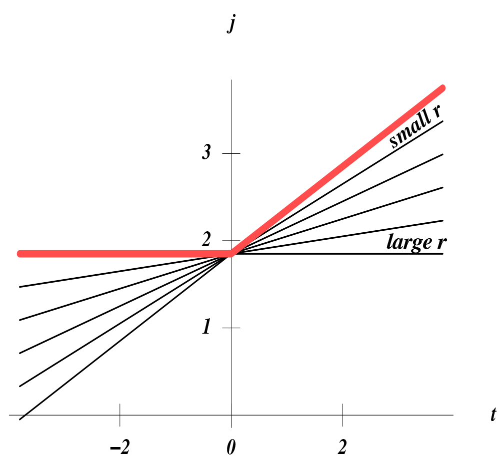

Fig. 8. The $N = 4$ SYM $I\!P$ trajectory which has different slopes at positive and negative t. The figure is taken from Brower, Polchinski, Strassler and Tan.

- Given a λ which is large enough, the total cross-section has a significant contribution from the diffraction dissociation channels originating mainly from the GW mechanism.
- Matching $N = 4$ SYM with pQCD [17], the self interaction of the Pomeron in $N = 4$ SYM is of the order of $2/\sqrt{\lambda}$. It is much smaller than the vertex of the hadron–$I\!P$–hadron, which is of the order of λ. Note that in the GLM model, the only contributing vertex is the

triple $I\!P$. This ingredient differentiates between GLM and the other $I\!P$ models discussed. The $I\!P$ parameters just estimated are in agreement with GLM fitted parameters.

I shall also quote 2 versions of the non-Pomeronic mini-jets model [18, 19]. These models, like DL, confine their investigation exclusively to the elastic channel and do not include diffraction in their analysis. As such, they disregard the GW mechanism. In my opinion, this is a serious deficiency shared also by the KP model.

7. The interface between theory and data

In this section I shall refer mostly to updated $I\!P$ models: GLM, KMR, KP and Os. These models share a basic approach, but they differ significantly in their modelings. In my opinion these differences can be traced, at lease in part, to the complexity of these model which is reflected in a large number of free parameters.

The four essential parameters which specify the main features of the Pomeron are $\Delta_{I\!P}$, $\alpha'_{I\!P}$, $G_{3I\!P}$ and γ, the low energy colorless dipole–target amplitude (alternatively we may refer to the p–$I\!P$–p vertex). Recall, though, that these are just four out of a large number of $I\!P$ model free parameters. Current Pomeron models adjust, out of necessity, their free parameters from the data analysis of relatively small data bases. This practical constraint was addressed differently by each of the quoted groups.

7.1. Data bases

GLM fit a data base of 58 points: $\sigma_{\rm tot}$, $\sigma_{\rm el}$, $\sigma_{\rm sd}$, $\sigma_{\rm dd}$ and $B_{\rm el}$ in the ISR–Tevatron range. We add a consistency check of SD forward slopes and CDF data on $\frac{d\sigma_{\rm el}}{dt}(t \leq 0.5~{\rm GeV}^2)$ and $\frac{d\sigma_{\rm sd}}{dtd(M^2/s)}(t = 0.05~{\rm GeV}^2)$. The wide energy range of this base necessitates the addition of a secondary Regge contribution.

KMR tune a smaller data base containing just the measured values of $\sigma_{\rm tot}$, $\frac{d\sigma_{\rm el}}{dt}(t \leq 0.5~{\rm GeV}^2)$ and $\frac{d\sigma_{sd}}{dtd(M^2/s)}(t = 0.05~{\rm GeV}^2)$. Os and KP tune a similar, somewhat larger, data base. KP did not specify their adjustment procedure. In this approach the integrated $\sigma_{\rm el}$, $\sigma_{\rm sd}$, and $\sigma_{\rm dd}$ are predicted rather than adjusted.

7.2. Adjustment of the free parameters

The incompatibility between the number of free parameters and size of the adjusted data base results with shortcuts and simplifications in the data analysis particular to each group.

The data analysis of GLM aims to simultaneously fit the 9 $I\!P$ and 5 Regge free parameters. We define $\sigma = \frac{1}{2}(\sigma(pp) + \sigma(\bar{p}p))$. Our fitted parameters are displayed in Table II. Our fit has χ^2/d.o.f.= 1.56. A very large contribution to the overall χ^2 stems from 2 $Sp\bar{p}S$ SD data points and CDF $\sigma_{\rm tot}$ at 1800 GeV. Neglecting these 3 points we obtain an excellent χ^2/d.o.f.= 0.86. Our fit provides a good reproduction of $\sigma_{\rm dd}$.

TABLE II

$\sigma_{\rm tot}$, $\sigma_{\rm rl}$, $\sigma_{\rm sd}$, $\sigma_{\rm dd}$ and S^2_H calculated by GLM, KMR, Kp and Os.

	1.8 TeV			7 TeV			14 TeV				100 TeV	
	GLM	KMR	Os	GLM	KMR	KP	GLM	KMR	Os	KP	GLM	KMR
$\sigma_{\rm tot}$	74.4	72.8	73.0	91.3	89.0	96.4	101.0	98.3	114.0	108.0	128.0	127.1
$\sigma_{\rm el}$	17.5	16.3	16.8	23.0	21.9	24.8	26.1	24.2	33.0	29.5	35.6	35.2
$\sigma_{\rm sd}$	8.9	11.4	9.6	10.2	15.4	12.0	10.8	17.6	11.0	14.3	12.7	24.7
$\sigma_{\rm dd}$	3.5	7.0	3.9	6.4		6.1	6.5	13.5	4.8	6.4	7.8	
S^2_H	0.11			0.06	0.024		0.04	0.015				

KMR, KP and Os data bases are predominantly sets of differential cross-sections. Such sets have a systemic behavior and, as such, it is non-trivial to obtain a significant "best fit" with a parameter rich model. KMR and Os assume (rather than adjust) the values of some parameters. Notably, they assume that $g_1 = g_2$. As we shall see, this choice determines the rate at which the elastic amplitude approaches the black disc bound.

There is a fundamental difference between the free parameter adjustment executed by GLM as compared with the procedure practiced by KMR and Os. GLM fit the complete data base, adjusting their model which is GW+$I\!P$-enhanced. KMR and Os factorize their tuning, adjusting the GW and non-GW sectors independently. Following Kaidalov, their diffraction is predominantly "high mass". In order to check the factorized procedure we have fitted our data base twice. Once using our procedure and once using the factorized one. The two sets of fitted parameter we have obtained are significantly different [20].

7.3. Diffractive low mass versus high mass

A systemic study of diffraction has to address a conceptual ambiguity. Whereas the definition and signature of elastic scattering are straight forward, there are no unambiguous definitions and signatures of soft diffraction. This problem is disturbing conceptually, and more, so practically. The lack of a uniformity introduces some level of ambiguity in the attempts to determine the energy dependence of soft diffractive channels.

GW original study incorporated the few known discrete nucleon isobar states as the diffractive component in their mechanism. Mueller's triple $I\!P$ approximation is valid when $s \gg M^2 \gg m_p$. The added "high mass" diffraction is continuous. Its common (arbitrary) high limit is $\frac{M^2}{s} \leq 0.05$. ISR experimental SD studies, at the time, used in most (but not all) of their publications a reasonable lower mass limit of 1.4 GeV^2. Their SD mass distribution above this limit is smooth.

Kaidalov, in his break-through studies of high energy diffraction, adopted the original GW point of view defining the GW diffracted mass to be $Y \leq 3$, corresponding to $M^2 \leq 4.5$ GeV^2. $Y > 3$ defines the non-GW "high mass". KMR, and Os adopt Kaidalov's original definitions. Note that with such a definition the smooth continuity of M is not maintained at $Y = 3$.

GLM offers a radically different approach in which GW diffraction has no Y cut, and it is continuous in M^2 up to 0.05 s. Multi $I\!P$ diagrams generating the non-GW diffraction are summed above $Y = 3$. The net result is that GLM diffraction has a significant GW component, whereas KMR and Os diffraction is predominantly non-GW. KP is a single channel model. As such, its SD is strictly "high mass". In the ISR–Tevatron range the difference between the two definitions is relatively small. At LHC energies the difference becomes significant.

7.4. Calculated cross-sections

Table III displays the output results of the soft cross-sections and central Higgs gap survival factor as calculated by the $I\!P$ models which are compatible with s and t unitarity.

TABLE III

GLM adjusted free parameters.

$\Delta_{I\!P}$	β	$\alpha'_{I\!P}$	g_1	g_2	m_1	m_2
0.2	0.388	0.020 GeV^{-2}	2.53 GeV^{-1}	88.4 GeV^{-1}	2.648 GeV	1.37 GeV
Δ_R	γ	α'_R	g_1^R	g_2^R	$R^2_{0,1}$	$G_{3I\!P}$
−0.466	0.0033	0.4 GeV^{-2}	14.5 GeV^{-1}	1343 GeV^{-1}	4.0 GeV^{-2}	0.0173 GeV^{-1}

- GLM, KMR and Os total, elastic and SD cross-sections are compatible at 1800 GeV.
- GLM and Os SD cross-sections are compatible. KMR are moderately larger at 1.8 TeV, increasing fast with energy.
- KMR $\sigma_{\rm dd}$ is consistently much larger. This may be considered as a signature of the KMR model.

- GLM and KMR total and elastic cross-sections are compatible over a remarkable energy range spanning 1.8 to 100 TeV.
- Os total and elastic predictions grow much faster than GLM and KMR, probably because of the hard $I\!P$ component of his model.
- KP $\sigma_{\rm tot}$ are larger than GLM and KMR.

Recall that, the main difference between the quoted models is in the formulation and summation procedures of their multi $I\!P$ sector which becomes significant at higher energies.

8. Exceedingly high energy behavior

The basic GW amplitudes of the GLM model are $A^{\rm S}_{1,1}$, $A^{\rm S}_{1,2}$ and $A^{\rm S}_{2,2}$. These are the building blocks with which we construct $a_{\rm el}$, $a_{\rm sd}$ and $a_{\rm dd}$ (3.21)–(3.23). The $A^{\rm S}_{i,k}$ amplitudes are bounded by s-channel unitarity black disc bound of unity. $a_{\rm el}(s,b)$ reaches this bound at a given (s,b) when, and only when, $A^{\rm S}_{1,1}(s,b) = A^{\rm S}_{1,2}(s,b) = A^{\rm S}_{2,2}(s,b) = 1$, independent of the value of β. Consequently, when $a_{\rm el}(s,b) = 1$, $a_{\rm sd}(s,b) = a_{\rm dd}(s,b) = 0$.

Checking GLM fitted parameters in Table III we observe that $g_2 \gg g_1$. As a consequence, the three basic GW amplitudes reach the black disc bound at different energies. The net result is that GLM approach toward the black disk bound is somewhat slower than in KMR and Os in which $g_1 = g_2$.

The behavior of the ratio $R_D(s) = \frac{\sigma_{\rm el}(s)+\sigma_{\rm sd}(s)+\sigma_{\rm dd}(s)}{\sigma_{\rm tot}(s)}$ conveys information on the onset of s-unitarity as a function of s. Assume that diffraction originates exclusively from the GW mechanism, we obtain the Pumplin bound [21] $R_D \leq 0.5$. The non-GW diffraction is not included in this bound as it originates from $G^{\rm in}_{i,k}$. Hence, the non-screened non-GW diffraction which is rising monotonically with energy is suppressed by by the LRG survival probability, which is decreasing with energy at a faster rate.

One should be careful when checking unitarity properties that are obtained from a b-integration. An interesting example is to check $\frac{\sigma_{\rm el}}{\sigma_{\rm tot}}$ at exceedingly high energy where the elastic amplitude is mostly black. Recall, though that this does not apply at the high b-tail where $a_{\rm el}(s,b) < 1$. As a consequence we have a very small, but non-zero diffractive cross-section. See Fig. 9.

9. LHC data and its interpretation

9.1. From the Tevatron to LHC

LHC preliminary data, relevant to this presentation, become available only recently. The phenomenological relevant predictions, obtained from either dynamical models or simulation Monte Carlo programs, are based on

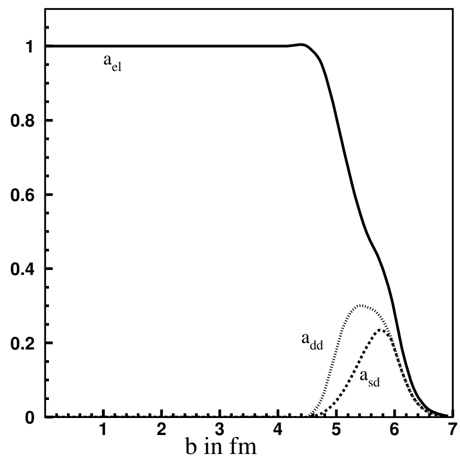

Fig. 9. GLM El, SD, and DD b-space amplitudes at the Planck scale.

relatively low energy data input. We have, thus, to consider a few essential issues:

1. A successful reproduction of the soft scattering data in the ISR–Tevatron range is a pre-requisite for a model or a simulation to be considered as a source of LHC predictions. As we noted, the Tevatron data, on its own, does not have the resolution to discriminate between models. Consequently, a successful reproduction of the Tevatron data does not secure a similar success at the LHC.

2. From a dynamical point of view, the question is if we have to consider some new dynamics above the Tevatron. Specifically, the analysis of the Tevatron soft scattering data is consistent with $I\!\!P$-enhanced dynamics, but not sufficient to verify it conclusively.

3. The condition for multi $I\!\!P$ dynamics to be significant depends on a delicate balance between $\Delta_{I\!\!P}$, $\alpha'_{I\!\!P}$, $G_{3I\!\!P}$ and γ. The analysis [8, 10] of the Tevatron soft scattering data implies a relevance of multi $I\!\!P$ interactions at the LHC.

4. In a very interesting presentation at this meeting, Rick Field compared the Tevatron and LHC inclusive pseudorapidity distributions $dN_{\rm ch}/d\eta$. His method was to check if Monte Carlo programs, which reproduced the CDF data well, could be tuned so as to fit the LHC new data at 7 TeV. Field's conclusion was that the tunes he checked under estimated the LHC data by 20–50%.

9.2. Inclusive pseudorapidity distributions

ALICE, CMS and ATLAS [23] have recently published the NSD charged multiplicity density

$$dN_{\mathrm{ch}}/d\eta = (1/\sigma_{\mathrm{NSD}})d\sigma/d\eta\,, \tag{9.39}$$

at central pseudorapidity $-2.5 \leq \eta \leq 2.5$. This data provides an additional angle to assess $I\!P$ models. The following is a short summary of the GLM approach. In the framework of Gribov's $I\!P$ calculus, single inclusive cross-sections can be calculated using Mueller diagrams [6] (see Fig. 10). In the

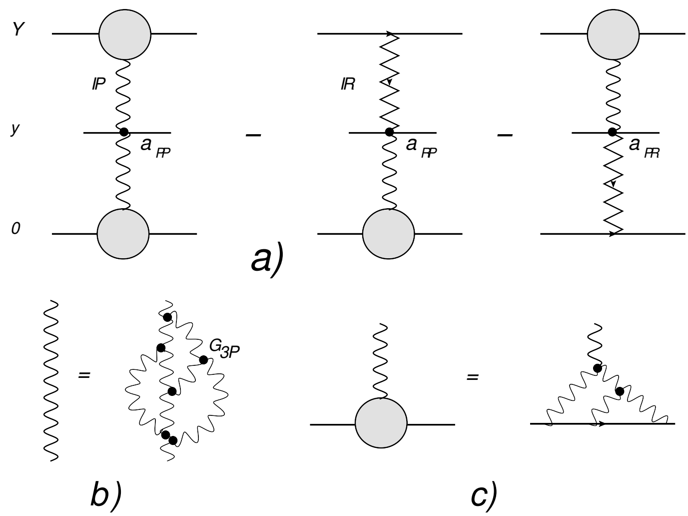

Fig. 10. (a) Mueller inclusive diagrams, (b) $I\!P$ Green function, (c) $I\!P$-hadron vertex. A bold waving line $= I\!P$. A zigzag line $= R$.

calculation, we have used the fitted parameters of the GLM $I\!P$ model, to which we have to add 3 additional phenomenological parameters [24]: $a_{I\!PI\!P}$ and $a_{I\!PR} = a_{RI\!P}$, which account for hadron emission from the $I\!P$ or Reggeon propagators. Q is the average transverse momentum of the produced mini-jets with a mass Q_0Q. In BNL mini-jets studies [25] $Q_0 = 2$ GeV.

The inclusive data fit depends, thus, on 3 free parameters. The data base for this fit is obtained from experiments spread over many years with different approaches to their cuts and error estimates. We have fitted the data twice. Once, fitting the 546, 900, 1800, 2369, 7000 GeV data [23, 26]. The second fit was confined to the very recent CMS data [23] at 900, 2360, 7000 GeV. The 2 sets of fitted parameters are close but not identical. In particular, the difference between the 2 values of Q/Q_0 is significant for the CMS fits at small η. See Table IV and Figs. 11 and 12.

TABLE IV

GLM fitted parameters for the two data sets of inclusive distributions.

Data	$a_{I\!PI\!P}$	$a_{I\!PR}$	Q_0/Q
CMS	0.390	0.186	0.427
All	0.413	0.194	0.356

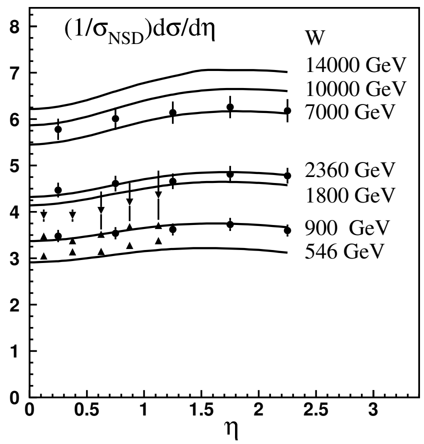

Fig. 11. GLM fit to inclusive charged pseudorapidity distributions. Data from Refs. [23, 26].

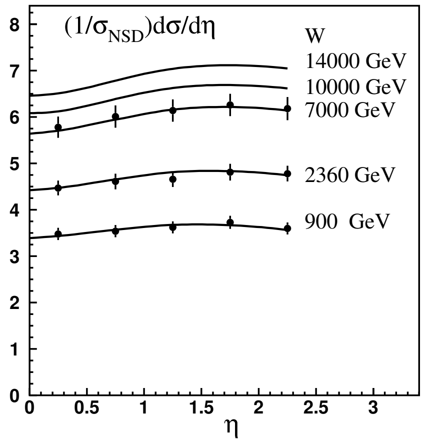

Fig. 12. GLM fit to CMS inclusive charged pseudorapidity distributions.

Our results are important in as much as we offer a simultaneous reproduction of the Tevatron and LHC data.

9.3. Inelastic cross-sections

Cross-sections contributing to $\sigma_{\rm tot}$ are

$$\sigma_{\rm tot} = \sigma_{\rm el} + \sigma_{\rm sd} + \sigma_{\rm dd} + \sigma_{\rm nd} = \sigma_{\rm el} + \sigma_{\rm inel}\,. \tag{9.40}$$

The first measurements of the inelastic cross-section derive from the minimum bias data samples. This procedure requires, though, an extrapolation aimed to include also high η tracks which are out of the detection acceptance.

$\sigma_{\rm inel}$ can be also determined as the difference $\sigma_{\rm inel} = \sigma_{\rm tot} - \sigma_{\rm el}$, provided both $\sigma_{\rm tot}$ and $\sigma_{\rm el}$ are measured. Regardless of the measuring procedure, $\sigma_{\rm inel}$ values at 7 TeV have been recently published by ALICE, ATLAS, CMS and TOTEM [27, 28].

$\sigma_{\rm inel}$ have been predicted by multi channel unitary models [8, 10, 12] and, also, by single channel models in which the GW mixing is ignored [11, 19, 18]. I shall discuss this issue in the discussion subsection.

Tables V and VI compare between LHC measured values of $\sigma_{\rm inel}$ at 7 TeV and five model predictions. The four experimental values of $\sigma_{\rm inel}$ are consistent. Note, though, that TOTEM's errors are considerably smaller. Within the experimental errors, the predicted $\sigma_{\rm inel}$ values are consistent with the data, even though they are consistently some what lower.

TABLE V

LHC $\sigma_{\rm inel}$ at 7 TeV.

ATLAS	ALICE	CMS	TOTEM
$69.4 \pm 2.4 \pm 6.9$	$72.7 \pm 1.1 \pm 5.1$	$71.8 \pm 1.1 \pm 2.0 \pm 7.9$	$73.5 \pm 0.6 + 1.8 - 1.3$

TABLE VI

$\sigma_{\rm inel}$ theoretical predictions.

Achilli *et al.*	Block–Halzen	GLM	Kaidalov–Poghosyan	KMR
60–75	69.0	68.3	70.0	62.6–67.1

9.4. Total and elastic cross-sections

Tables VII presents the LHC values [28, 29] of $\sigma_{\rm tot}$ and $\sigma_{\rm el}$. A sample of the corresponding predictions [19, 18, 8, 11, 10] are presented in Table VIII. As seen, the predictions of KP and Block–Halzen are compatible with the data while GLM and KMR are systematically lower.

TABLE VII

LHC $\sigma_{\rm tot}$ and $\sigma_{\rm el}$.

	TOTEM	ATLAS	CMS
$\sigma_{\rm tot}$ mb	$98.3 \pm 0.2 \pm 2.7 + 0.8 - 0.2$	$96.0 \pm 3.3 \pm 9.5$	$94.0 \pm 2.8 \pm 5.5$
$\sigma_{\rm el}$ mb	$24.8 \pm 0.2 \pm 2.8$	26.6	22.2

TABLE VIII

$\sigma_{\rm tot}$ and $\sigma_{\rm el}$ theoretical predictions.

	Achilli *et al.*	Block–Halzen	GLM	KP	KMR
$\sigma_{\rm tot}$ mb	91.6	95.4	91.3	96.4	89.0
$\sigma_{\rm el}$ mb		26.4	23.0	24.8	21.9

9.5. Discussion

A comparison between the presently available LHC soft cross-sections with the corresponding theoretical predictions (Tables V–VIII) leads to a few observations:

- The 7 TeV total cross-section predictions of GLM and KMR, are lower than the LHC data, which are well reproduced by Block–Halzen and KP. Note that, all $\sigma_{\rm tot}$ values obtained by the LHC groups are larger than the DL prediction [3] of 90.7 mb. See also Ref. [30].
- Block–Halzen and Achilli *et al.* are non-Pomeronic single channel mini-jets models, which refrain from discussing diffraction. In my opinion this is a major deficiency of these models. Recall also that single channel models are prone to produce relatively large survival probabilities. Indeed, S^2 calculated by Refs. [18,19] are considerably higher than the GLM and KMR S^2 estimates which are compatible with the Tevatron di-jets data.
- KP is a single channel $I\!\!P$ model *i.e.* its diffraction is exclusively "high mass". This is in disagreement with a recent analysis of LHC data by KMR [30] in which $\sigma_{\rm sd}^{{\rm low}\,M}$ was estimated to be 7–10 mb. An additional deficiency of KP is that this is a model with 4 trajectories. As such, it depends on exceedingly high number of free parameters in no proportion to the size of its adjusted data base.
- Considering the above, an assessment of the necessity of advanced Pomeron model phenomenology in the analysis of LHC soft scattering data remains opened. Both GLM and KMR can improve their output with a careful tune of their parameters. The issue at stake, though, is the exclusivity of this option.

I wish to thank my long time collaborators E. Gotsman and E. Levin for a constructive and enjoyable partnership. Special thanks are due to Prof. Michał Praszałowicz and his team for a splendid and most friendly organized summer school.

REFERENCES

[1] G.F. Chew, S. Frautschi, *Phys. Rev.* **123**, 1478 (1961).

[2] V.N. Gribov, *Sov. Phys. JETP* **15**, 873 (1962); *Sov. Phys. JETP* **26**, 414 (1968); *Sov. J. Nucl. Phys.* **9**, 369 (1969).

[3] A. Donnachie, P.V. Landshoff, *Nucl. Phys.* **B231**, 189 (1984); *Phys. Lett.* **B296**, 227 (1992); *Zeit. Phys.* **C61**, 139 (1994).

[4] M.L. Good, W.D. Walker, *Phys. Rev.* **120**, 1857 (1960).

[5] A.B. Kaidalov, L.A. Ponomarev, K.A. Ter-Martirosyan, *Sov. J. Nucl. Phys.* **44**, 468 (1986).

[6] A.H. Mueller, *Phys. Rev.* **D2**, 2963 (1970); *Phys. Rev.* **D4**, 150 (1971).

[7] E. Gotsman, E. Levin, U. Maor, *Phys. Lett.* **B452**, 387 (1999); *Phys. Rev.* **D60**, 094011 (1999).

[8] E. Gotsman, E. Levin, U. Maor, *Eur. Phys. J.* **C71**, 1553 (2011); *Eur. Phys. J.* **C71**, 1685 (2011).

[9] A.H. Mueller, B. Patel, *Nucl. Phys.* **B425**, 471 (1994); A.H. Mueller, G.P. Salam, *Nucl. Phys.* **B475**, 293 (1996); G.P. Salam, *Nucl. Phys.* **B461**, 512 (1996); E. Iancu, A.H. Mueller, *Nucl. Phys.* **A730**, 460 (2004).

[10] V.A. Khoze, A.D. Martin, M.G. Ryskin, *Eur. Phys. J.* **C71**, 1617 (2011).

[11] A.B. Kaidalov, M.G. Poghosyan, `arXiv:0909.5156v1 [hep-ph]`; *Eur. Phys. J.* **C67**, 397 (2010); `arXiv:1109.3697v1 [hep-ph]`.

[12] S. Ostapchenko, *Phys. Rev.* **D83**, 014018 (2011); *Phys. Rev.* **D81**, 114028 (2010).

[13] F.E. Low, *Phys. Rev.* **D12**, 163 (1975); S. Nussinov, *Phys. Rev. Lett.* **34**, 1286 (1975).

[14] E. Gotsman, E. Levin, U. Maor, *Eur. Phys. J.* **C71**, 1685 (2011).

[15] F.S. Fadin, E.A. Kuraev, L.N. Lipatov, *Phys. Lett.* **B60**, 50 (1975); E.A. Kuraev, L.N. Lipatov, F.S. Fadin, *Sov. Phys. JETP* **44**, 443 (1977); *Sov. Phys. JETP* **45**, 199 (1977); Ya.Ya. Balitsky, L.N. Lipatov, *Sov. J. Nucl. Phys.* **28**, 822 (1978).

[16] R.C. Brower, J. Polchinski, M.J. Strassler, C.I. Tan, *J. High Energy Phys.* **0712**, 005 (2007); R.C. Brower, M.J. Strassler, C.I. Tan, *J. High Energy Phys.* **0903**, 092 (2009); *J. High Energy Phys.* **0903**, 050 (2009); R.C. Brower, M. Djuric, J. Sarcevic, C.I. Tan, *J. High Energy Phys.* **1011**, 051 (2010).

[17] J. Bartels, C. Ewerz, *J. High Energy Phys.* **9909**, 026 (1999).

[18] M. Block, F. Halzen, *Phys. Rev.* **D83**, 077901 (2011).

[19] A. Achilli *et al.*, `arXiv:1102.1949v3 [hep-ph]`.

[20] E. Gotsman, E. Levin, U. Maor, J.S. Miller, `arXiv:0903.0247v1 [hep-ph]`.

[21] J. Pumplin, *Phys. Rev.* **D8**, 2249 (1973).

[22] CDF Collaboration, *Phys. Rev.* **D50**, 5535 (1994).

[23] ALICE Collaboration, *Eur. Phys. J.* **C65**, 111 (2010); CMS Collaboration, *J. High Energy Phys.* **1002**, 041 (2010); ATLAS Collaboration, `arXive:1003.3124[hep-ph]`.

[24] E. Gotsman, E. Levin, U. Maor, to be published in *Phys. Rev.* **D** (2011).

[25] D. Kharzeev, E. Levin, *Phys. Lett.* **B523**, 79 (2001).

[26] C. Amsler *et al.*, *Phys. Lett.* **B667**, 1 (2008).

[27] M. Poghosyan [ALICE Collaboration], `arXiv:1109.4510v1 [hep-ex]`; ATLAS Collaboration, `arXiv:1104.0326v1 [hep-ex]`; CMS Collaboration, CMS PASFWD-11-001, CERN/Record 1373466 (2011).

[28] TOTEM Collaboration, `arXiv:1110.1395v1 [hep-ex]`.

[29] Quoted in F. Halzen *et al.*, RIKEM-MP-27 (2011), `arXiv:1110.1479v1 [hep-ph]`.

[30] A.D. Martin, M.G. Ryskin, V.A. Khoze, `arXiv:1110.1973v1 [hep-ph]`.